



POLITECNICO DI TORINO  
Repository ISTITUZIONALE

Mechanical properties of microcrystalline branching selenite gypsum samples and influence of constituting factors

*Original*

Mechanical properties of microcrystalline branching selenite gypsum samples and influence of constituting factors / Caselle, C.; Bonetto, S.; Colombero, C.; Comina, C.. - In: JOURNAL OF ROCK MECHANICS AND GEOTECHNICAL ENGINEERING. - ISSN 1674-7755. - ELETTRONICO. - 11:2(2019), pp. 228-241.

*Availability:*

This version is available at: 11583/2742628 since: 2019-07-17T18:25:22Z

*Publisher:*

Chinese Academy of Sciences

*Published*

DOI:10.1016/j.jrmge.2018.09.003

*Terms of use:*

openAccess

This article is made available under terms and conditions as specified in the corresponding bibliographic description in the repository

*Publisher copyright*

(Article begins on next page)



Contents lists available at ScienceDirect

# Journal of Rock Mechanics and Geotechnical Engineering

journal homepage: [www.rockgeotech.org](http://www.rockgeotech.org)

Full Length Article

## Mechanical properties of microcrystalline branching selenite gypsum samples and influence of constituting factors

C. Caselle<sup>a,\*</sup>, S. Bonetto<sup>a</sup>, C. Colombero<sup>b</sup>, C. Comina<sup>a</sup><sup>a</sup>Department of Earth Sciences (DST), Università degli Studi di Torino, Torino, 10125, Italy<sup>b</sup>Department of Environment, Land and Infrastructure Engineering (DIATI), Politecnico di Torino, Torino, 10129, Italy

## ARTICLE INFO

## Article history:

Received 26 March 2018

Received in revised form

23 July 2018

Accepted 4 September 2018

Available online 3 December 2018

## Keywords:

Gypsum

Uniaxial compressive strength (UCS)

Point load test (PLT)

Mechanical properties

Geological heterogeneity

## ABSTRACT

The high sedimentological variability of gypsum rocks has the effect that a univocal characterization of this material is not easy to establish. This is particularly true from the geomechanical point of view: when the mechanical properties of gypsum rocks are requested, it is therefore necessary to undertake detailed characterization analyses. Common facies of gypsum was observed in the Upper Miocene evaporitic succession (Messinian Salinity Crisis) within the whole Mediterranean Basin. In this work, mechanical tests were conducted on a site-specific facies, represented by the microcrystalline branching selenite. The tested samples came from the Monferrato area (northwestern Italy). Uniaxial compressive strength (UCS) tests were performed in order to obtain reference mechanical parameters. More rapid and economic point load test (PLT) and ultrasonic pulse velocity (UPV) measurements were additionally performed to verify their applicability as complementary/alternative methods for site characterization. Rock-type specific PLT-UCS and UPV-UCS relationships were established. A wide dispersion of the mechanical parameters was observed due to the heterogeneities of the studied material. Consequently, compositional, textural and microstructural observations on selected samples were performed. Two main material classes were recognized based on average grain size and total gypsum content, underlining the significant influence of the grain sorting on the measured mechanical properties.

© 2019 Institute of Rock and Soil Mechanics, Chinese Academy of Sciences. Production and hosting by Elsevier B.V. This is an open access article under the CC BY-NC-ND license (<http://creativecommons.org/licenses/by-nc-nd/4.0/>).

### 1. Introduction

Rock mass classification and geotechnical design in mining industry and rock-related structures require definition of specific geotechnical parameters, providing a strength indication for the studied material (e.g. shear resistance and compressive strength). One of the most widely used parameters in various engineering issues, including the selection of appropriate excavation techniques and stability analyses, is the uniaxial compressive strength (UCS). Destructive tests, traditionally used to estimate UCS, are however expensive and need accurate sample preparation. This often results in a small set of tested samples, which could not be adequate in number to account for the high geological variability of the studied material. Consequently, cheaper and faster methodologies, providing alternative physical and mechanical parameters

potentially correlated with UCS, have been proposed by various authors (among others, Hatherly et al., 2007; Sharma and Singh, 2008; Lawrence et al., 2013).

The simplest method to provide an expeditious index of the rock mechanical strength is the point load test (PLT). This technique is economic and quick; it does not require any specimen preparation and can be carried out directly on site. By contrast, deformation is not controlled during the test. The resulting PLT strength index  $I_{550}$  can be potentially correlated with UCS (ISRM, 1985; ASTM D5731-07, 2007). Different authors focused on rock-type dependent  $I_{550}$ -UCS relationships and conversion factors (Broch and Franklin, 1972; Bieniawski, 1975; Chau and Wong, 1996; Hardy, 1997; Tsiambaos and Sabatakakis, 2004; Fener et al., 2005; Kahraman et al., 2005; Çobanoğlu and Çelik, 2008; Kahraman and Gunaydin, 2009; Basu and Kamran, 2010; Singh et al., 2012; JahanGer and Ahmed, 2013; Li and Wong, 2013; Salah et al., 2014; Kaya and Karaman, 2015; Akram et al., 2017; Liu et al., 2017; Everall and Sanislav, 2018).

Besides destructive methods, non-destructive ultrasonic tests can be used to indirectly assess the rock mechanical properties, by correlations between ultrasonic pulse velocity (UPV) and elastic or

\* Corresponding author.

E-mail address: [chiara.caselle@unito.it](mailto:chiara.caselle@unito.it) (C. Caselle).

Peer review under responsibility of Institute of Rock and Soil Mechanics, Chinese Academy of Sciences.

strength parameters (McNally, 1990; Yasar and Erdogan, 2004; Hatherly et al., 2005; Oyler et al., 2010). In particular, UPV-UCS correlations were recently established for different rock types in several studies (Vasconcelos et al., 2008; Butel et al., 2014; Karaman and Kesimal, 2015; Wang and Li, 2015; Zel et al., 2015; Colombero et al., 2016; Vasanelli et al., 2017).

Following these approaches, an integration of the most established destructive techniques (UCS) with faster and cheaper methodologies (PLT and UPV) is presented in this work to obtain appropriate correlations and a reliable technical characterization of a specific facies of gypsum. Even if relatively standard methodologies have been applied in this work, similar approaches are not available in the literature on branching selenite. New specific material-calibrated relationships are therefore proposed with the aim of improving geotechnical design over similar facies of gypsum. An innovative classification based on compositional, textural and microstructural observations is additionally proposed which could be helpful in discriminating this particular facies behavior. Gypsum rock observed in nature shows indeed a large variety of ages, formation mechanisms, depositional environments and facies. Each type of gypsum is marked by specific features in terms of grain size, texture, microstructure and composition (Lugli et al., 2010).

Previous studies were accomplished on the mechanical properties of specific gypsum facies. Papadopoulos et al. (1994) compared the mechanical properties of alabastrine, medium-grained and coarse-grained Neogene gypsum from Crete, recognizing the underlying strong influence of formation mechanisms and depositional environments. Yilmaz and Sendir (2002) analyzed the relationships of Schmidt rebound number with UCS and Young's modulus ( $E_t$ ) on a pure alabastrine gypsum type from the Sivas Basin (Turkey); whereas the mechanical properties of porphyric and alabastrine gypsum types from the same basin were compared in Yilmaz (2007). At the nanoscale, Chen et al. (2010) analyzed the flexural strength of individual crystal of gypsum and its influence on the elastic properties of specific geometrical configuration of crystal agglomerates at high porosities (needle aggregates and homogeneous randomly oriented single crystals) to study synthetic samples. Heidari et al. (2012) proposed PLT-UCS correlations for a specific gypsum facies from the Early Miocene Gachsaran Formation (Iran), with peculiar crystalline-gypsum and micrite layers and veins. The above-mentioned works and resulting correlations have however to be considered valid only for the particularly analyzed facies.

Recently, sedimentologists underlined the presence of a specific facies, named branching selenite, in most of the Upper Miocene evaporites of the Mediterranean Basin (Lugli et al., 2010). This facies has a scientific and economic significance because it is associated with a specific layer (reported in geological literature as "key layer") and consequently very useful for both stratigraphic studies and ore body reconstructions for mining. Despite its importance, mechanical investigations and specific correlations for this specific facies are not available in the literature and are therefore worthy of investigation.

Branching selenite, as well as some other gypsum facies, is commonly exploited in either open pits or underground quarries. Mining tunnels in gypsum formations can reach lengths of tens of kilometers, and thus both underground and surface stabilities have to be assured. Nevertheless, in everyday practice, the lack of a specific focus on the relationship between gypsum geological variability and strength parameters often leads to ignoring of important information for the mechanical characterization of the ore deposits.

The present research focuses on the mechanical characterization of a set of branching selenite samples coming from the Monferrato area (northwestern Italy). Special attention is paid to correlations among different mechanical tests that have to be facies-specific, in reason of the described high geological variability of gypsum rocks. Results of destructive (UCS and PLT) and non-destructive (UPV) tests

on branching selenite samples and facies-specific correlations among them are reported. The possibility to complement the mechanical characterization obtained from UCS tests with a larger number of cheaper and more expeditious tests, such as PLT and UPV, resulted in a much larger available dataset without significant cost increase. Because of the wide dispersion in the collected mechanical parameters observed within the same gypsum facies, further chemical (i.e. gypsum content) and physical (i.e. rock texture and microstructure) characterizations of the tested rock samples were undertaken. As a matter of fact, the strength dependence from geological and physical features, such as grain size and mineralogy, has been suggested by many authors for several other rock types (Aggitalis et al., 1980; Hatzor and Palchik, 1997; Palchik and Hatzor, 2004; Tsiambaos and Sabatakakis, 2004; Kahraman et al., 2005; Sabatakakis et al., 2008; Rajabzadeh et al., 2012; Weng and Li, 2012; Ju et al., 2013; Karakul and Ulusay, 2013; Wasantha et al., 2015; Aladejare and Wang, 2017; Yu et al., 2017).

## 2. Geological framework

During the Messinian Salinity Crisis, both hyper-haline and hypo-haline sediments were deposited all over the Mediterranean basin, in three successive phases (Lugli et al., 1999; Dela Pierre et al., 2002, 2007, 2011, 2012, 2014; Roveri et al., 2008; Manzi et al., 2009, 2011, 2013). During the first phase (5.971–5.60 Ma), the primary lower gypsum (PLG) Unit was deposited in the marginal basins, while anoxic marls settled in the deeper basins. The second phase (5.60–5.55 Ma) corresponded to the resedimentation of the PLG Unit as a chaotic body (resedimented lower gypsum (RLG)) in the deeper basins. Eventually, during the third phase (5.55–5.33 Ma), hypo-haline sediments in the so-called "Lago-Mare" facies were locally deposited. The resulting distribution of Messinian evaporitic sediments in the Mediterranean basin is shown in Fig. 1.

The organization of sediments within the PLG Unit is cyclically dependent on the influence of orbital parameters on the paleoclimatic conditions. Within the unit, it is possible to recognize pairs of gypsum and marl layers which are usually repeated in a cyclical way. Even if the beginning of gypsum deposition is not synchronous in the entire Mediterranean basin, several studies allowed to identify the stratigraphic beginning of the salinity crisis, even where the

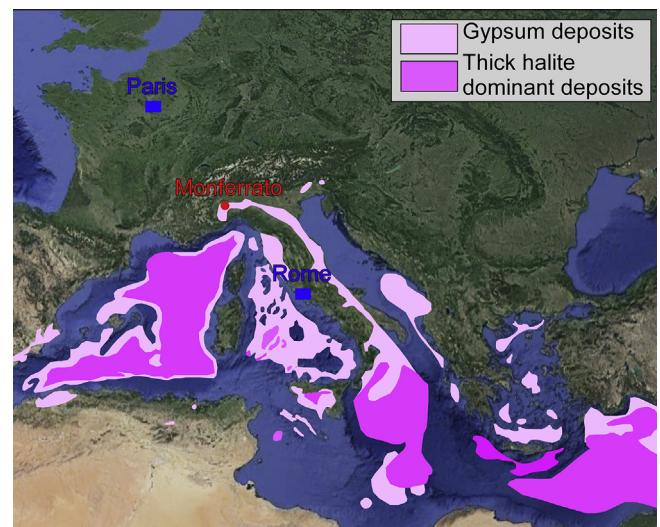


Fig. 1. Distribution of Messinian evaporites in the Mediterranean basin (modified from Rouchy and Caruso, 2006). The sampling area for the gypsum rock facies of the present study is highlighted in red (Monferrato, northwestern Italy).

gypsum was not yet deposited (Hilgen et al., 1995; Manzi et al., 2013). A total number of 16 marl–gypsum cycles were recognized.

According to Lugli et al. (2010), different facies are observed in the PLG Unit of the whole Mediterranean area: giant and massive selenite, banded selenite, branching selenite, displacive selenite, gypsarenite and gypsrudite.

The *giant and massive selenite* consists of twinned gypsum crystals (called arrow-head or swallow-tail) with average size of several centimeters. The peculiar organization of these crystals was successfully used to determine the strata polarity in mining operation, because the vertical crystal growth direction is sub-perpendicular to the stratification.

The *banded selenite* or grass-like selenite consists of relatively small vertical crystals, less than 10 cm in thickness, which are separated by thin few-millimeter thick carbonate laminae.

The *branching selenite* has been described as “nodular and lenticular selenite” or “wavy, needle-like selenite layers” (in Sicily, Italy) or “hemi-radial to radial selenite” (in Spain). It consists of clear selenite crystals, with length varying from some millimeters up to few centimeters, having their long axis inclined or oriented horizontally, grouped into decimeter-large irregular nodules and lenses separated by thin fine-grained carbonate or gypsum laminae. The crystal arrangement reveals that clusters of selenite grew laterally, grouped in branches, projecting outward from an initial nucleation zone into a fine-grained gypsum matrix resulting in a conical shape. Those cones are difficult to recognize because they are widely spaced and very broad so that the nucleation points are not always visible. The matrix surrounding the cones may consist mostly of gypsum or mudstone with fine-grained gypsum. This facies appears only from the 6th cycle and consequently allows an easy identification of this cycle over the whole Mediterranean basin. For this reason, the 6th cycle is considered as a key sedimentological level and is reported in the literature (Dela Pierre et al., 2011) as “Sturani Key Bed” (SKB).

The *displacive selenite* usually shows lenticular crystals, but a few twinned crystals have also been observed, up to 1 m across. They are commonly present above selenite beds, in contact with the overlying shale layers. The typical horizontal growth (“flat-laying”) of the lenticular crystals is opposed to the vertical growth of the primary selenite twins, and as in this case, the free space of the displacive growth is only horizontal because the shale layers are normally only a few decimeters thick.

The *gypsarenite* and *gypsrudite* are clastic deposits locally recognized throughout the selenite successions of the PLG Unit. They are limited to thin layers in the more marginal successions. In most of the cases, the selenite clasts are only slightly corroded, suggesting local erosion and deposition as a consequence of floods at the basin margins.

All these facies have been recognized in the evaporitic successions of the Mediterranean region, including the Monferrato geological domain (northwestern Italy), where samples for this study were collected (Clari et al., 1995; Piana and Polino, 1995). The Monferrato stratigraphic sequence (Fig. 2) shows that, under the SKB (6th cycle), three layers of massive selenite (10–12 m in thickness) are divided by marl layers with a thickness of approximately 2 m. The SKB layer has an average thickness of 10 m and it is mainly made of branching selenite with local banded-selenite facies. Over the SKB layer, finer interbedded layers of gypsum and marl are present, referred to as “higher evaporitic cycles” (Dela Pierre et al., 2016).

**3. Materials**

A total of 60 gypsum samples in branching selenite facies were obtained from 10 boreholes in the evaporitic succession of the Monferrato area. Core drilling on site was performed in vertical

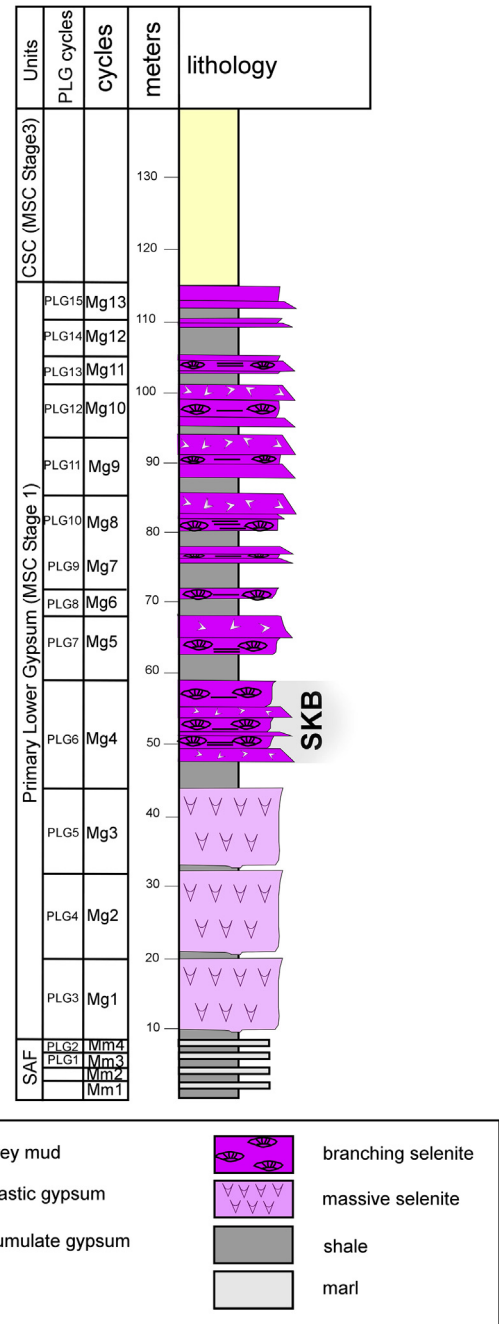


Fig. 2. Typical stratigraphic section of Messinian evaporitic deposits in the Monferrato area (Bernardi, 2013).

direction, i.e. perpendicularly to the sub-horizontal stratification and to the main sedimentary discontinuities. As a result, the axial direction of the cores is perpendicular to the stratigraphic anisotropy, which in the tested samples consists of carbonate or gypsum laminae embedded between homogenous nodules of gypsum crystals. In the studied area, stratification lies nearly horizontally and, in case of underground quarries, drifts run completely into the gypsum layers; the direction of maximum load on walls and pillars is therefore perpendicular to the sedimentary discontinuities. Consequently, UCS tests with uniaxial stress oriented normally to the sample anisotropies simulate on-site pillar conditions. For these reasons, PLT and UPV measurements were also performed in the same direction. Cores were made available from a private company and the related

diameter (80 mm) was out of our control. Final lengths of the selected cores, after parallel edge cutting with a circular saw (perpendicularly to core axis), were in the range between 200 mm and 500 mm. Number and size of the cores tested for mechanical characterization (UCS, PLT and UPV) are summarized in Table 1. The sampling procedure for each method is shown in Fig. 3. All cores were tested in dry conditions in order to reduce the additional influence of water content on the retrieved parameters.

Even if all the cores were tested with the non-destructive UPV technique, only 49 measurements are discussed in the following; the results of the remaining 11 cores were excluded due to the high standard deviation observed among the measurements.

For the destructive tests (UCS and PLT), in some cases, the total core length was higher than the standard required sample size. Therefore, these cores were further cut into shorter samples.

Gypsum content measurements and thin section observations were carried out on broken samples of PLT and UCS tests. In particular, 15 samples were devoted to the evaluation of the gypsum content and six samples to the preparation of thin sections.

Independent data from the same gypsum layer report an average porosity in the range between 4% and 8% and an average bulk weight of 22 kN/m<sup>3</sup>.

### 4. Methods

#### 4.1. Ultrasonic pulse velocity tests

UPV measurements were performed with an ultrasonic pulse generator Pundit (Proceq) which provides emission and acquisition (at a sampling frequency of 2 MHz) of P-waves by means of two cylindrical transducers having a nominal frequency of 54 kHz. Measurements were conducted following the requirements of ASTM D2845-08 (2008) for laboratory determination of pulse velocities. Particularly, all the investigated travel distances  $H$  (i.e. core length, 200–500 mm) obey the standard relationship with the minimum lateral dimension  $\phi$  (i.e. core diameter, 80 mm) and the average sample grain size  $d$ :

$$H \leq 5\phi \tag{1}$$

$$H \geq 10d \tag{2}$$

Branching selenite gypsum is a fine-grained rock having a maximum grain size of about 10 mm, thus investigated  $H$  basically obeys Eq. (2). Given the relatively low nominal frequency of the transducers, some discrepancies from the standard arose with the core diameters  $\phi$ , considering:

$$\phi \geq 5\lambda \geq 15d \tag{3}$$

where  $\lambda$  is the pulse wavelength, defined as

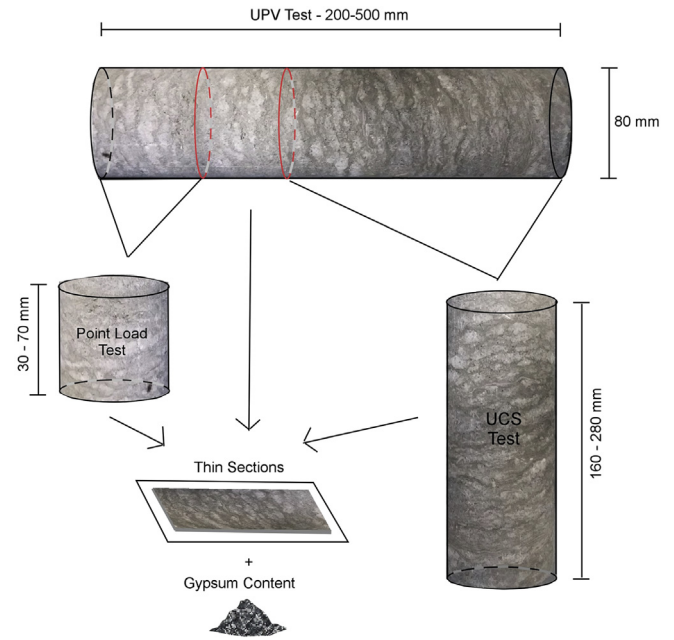


Fig. 3. Schematic representation of sample extraction from the long cores and preparation according to geometrical requirements of the five test methods.

$$\lambda = \frac{UPV}{f} \tag{4}$$

where  $f$  is the nominal frequency of the instrument (54 kHz). Considering an approximate average UPV of 2000 m/s, the expected wavelength  $\lambda$  is 37 mm. As a consequence, samples with diameter of 80 mm could not fully satisfy Eq. (3), but it was at least ensured to have measurements on samples obeying  $\phi > 2\lambda$ .

An average of ten UPV acquisitions was repeated on each sample. Manual picking of the first arrival times was performed on each recorded trace, to obtain the time of travel within the investigated core. Determination of the P-wave velocity was then straightforward since travel distances (core lengths) were known. Final UPV values for each sample were averaged over the 10 related measurements.

#### 4.2. Point load test

Gypsum samples were loaded in the PLT apparatus between two conical steel points, according to the suggested method for determining point load strength (ISRM, 1985; ASTM D5731-07, 2007). In test conditions involving core specimens tested along the axial direction, the sample geometric requirements follow:

Table 1  
Number of samples tested with the described methodologies and sizes of the specimens.

Test	Number of samples	Specimen sizes (length × diameter) (mm × mm)	Number of common samples
UPV test	49	(200–500) × 80	UCS-UPV: 15
PLT	35 (54 specimens)	(30–70) × 80	UCS-PLT: 8
UCS test with constant strain rate	8	(160–280) × 80	
UCS test with constant stress rate	9	(160–280) × 80	
Gypsum content measurement	15		UCS-gypsum content: 8 PLT-gypsum content: 13 (17 specimens)
			UPV-gypsum content: 12
Thin section observation	6		UCS-thin section: 4 PLT-thin section: 5 (8 specimens) UPV-thin section: 6

$$0.3\phi < H < \phi \quad (5)$$

For this reason, the cores were cut into smaller samples, with lengths between 30 mm and 70 mm (Table 1).

The point load index  $I_S$  is defined as the ratio between the applied force at failure ( $P$ ) and the equivalent diameter of the core ( $D_e$ ):

$$I_S = \frac{P}{D_e^2} \quad (6)$$

where

$$D_e^2 = \frac{4H\phi}{\pi} \quad (7)$$

Due to the influence of the sample diameter on  $I_S$ , a normalized value referred to as an equivalent sample with diameter of 50 mm ( $I_{S50}$ ) is used:

$$I_{S50} = \left(\frac{D_e}{50}\right)^{0.45} I_S \quad (8)$$

#### 4.3. Uniaxial compressive strength test

The UCS test is used for determination of the maximum strength and elastic parameters (Young's modulus and Poisson's ratio) of intact rock cores in uniaxial compression. Following ASTM D3148-02 (2002) and UNI EN 1926–2007 (2007), samples with geometrical features obeying Eq. (9) were placed in a loading frame and the axial load was continuously increased until failure:

$$2\phi < H < 2.5\phi \quad (9)$$

Both constant stress rate and constant strain rate tests were performed. In the first configuration, a mechanical (Comazzi) and a hydraulic (Galdabini) press were used for peak loads lower and higher than 50 kN, respectively. Only the maximum strength value was recorded, without strain measurement. In the second configuration, a constant deformation rate of 0.55  $\mu\text{m/s}$  was applied by means of a servo-controlled press; axial and lateral deformations were monitored throughout the test and the material behavior after the peak was also recorded. Local strains, in both axial and lateral directions, were measured using electrical resistance strain gages. To evaluate the reliability of this device, the total deformation of the sample in axial direction was also measured by means of linear variable differential transformers (LVDTs) on the steel plate of the press.

The UCS of each sample was expressed as the ratio of the failure load ( $F$ ) of the specimen to its cross-sectional area before testing ( $A$ ):

$$UCS = \frac{F}{A} \quad (10)$$

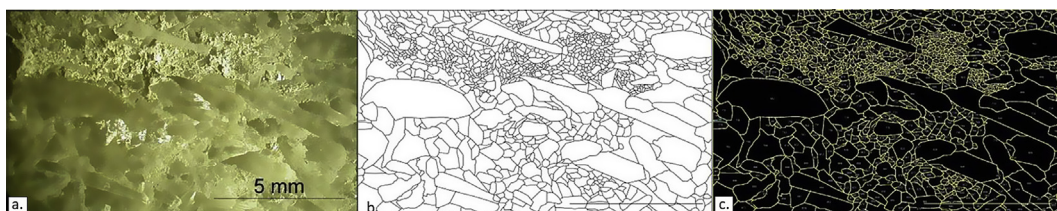


Fig. 4. (a) Representative area of the thin section of sample c (see Fig. 14); (b) Manually delineated edges of the grains; and (c) Calculated grain areas with the software ImageJ.

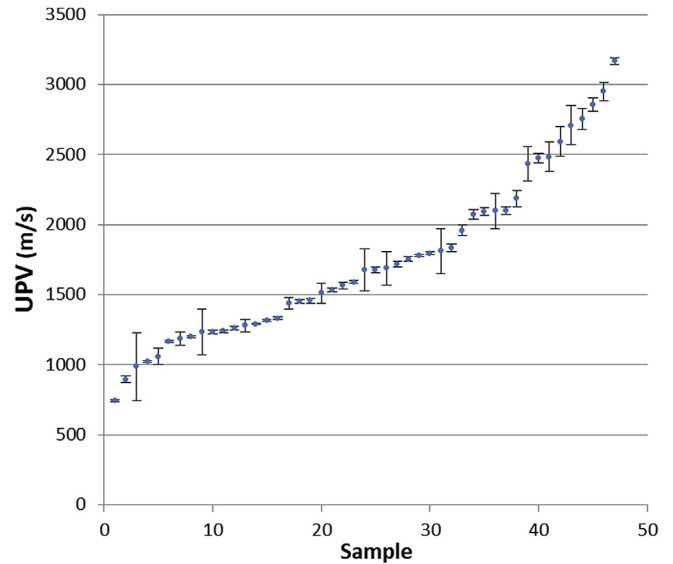
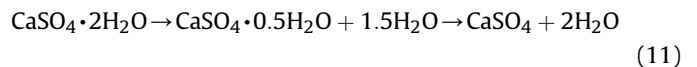


Fig. 5. Average UPV measurements on 49 samples, sorted in ascending order. The vertical black bars show the standard deviation of the ten measurements performed on each sample.

#### 4.4. Gypsum content measurement

The gypsum content in the samples was measured through the thermogravimetric method (Porta, 1998), which is based on the measure of the mass losses occurring during the heating of a sample due to the dehydration of gypsum. Calcium sulphate occurs in nature in the form of three different minerals distinguished by the degree of hydration: gypsum ( $\text{CaSO}_4 \cdot 2\text{H}_2\text{O}$ ), bassanite ( $\text{CaSO}_4 \cdot 0.5\text{H}_2\text{O}$ ) and anhydrite ( $\text{CaSO}_4$ ). The phase transition between these minerals depends on the temperature, following:



When the sample is heated to 105 °C, part of the gypsum crystal water is lost, and bassanite is produced. With increasing temperatures, all the gypsum is transformed into anhydrite; the total conversion is attained at about 200 °C. Knowing that the total amount of crystal water is 20.91% of the gypsum mass (Eswaran and Gong, 1991), from the measure of the sample mass variation during the heating, the gypsum percentage (mass) is obtained.

#### 4.5. Thin section observation

Given the heterogeneity of the facies, thin sections were prepared perpendicularly to the observed anisotropy (according to the loading direction). Large transparent glass supports (100 mm  $\times$  60 mm) were used for thick, smooth and polished slices of material (around 1 mm), to investigate representative portions of the samples. Cross-sections were then observed and described with

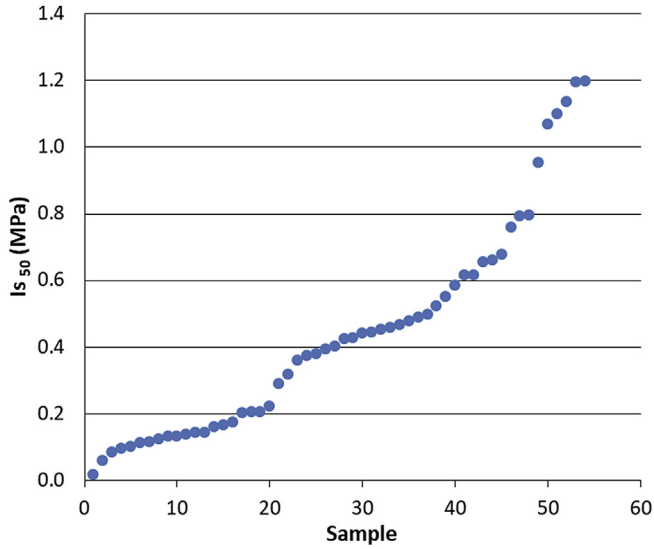


Fig. 6.  $I_{S50}$  values determined on 54 samples from point load test, sorted in ascending order.

optical microscope in reflected light to analyze texture and microstructures. The grain size distribution was quantitatively estimated with a photographic method. For each section, a representative area was selected and the inner grain edges were manually delineated. The area of the grains was retrieved with the software ImageJ and used to calculate the grain size distribution curves. An example of this image processing is shown in Fig. 4.

5. Results

5.1. Ultrasonic pulse velocity test

The average UPV values obtained on the 49 samples are reported in Fig. 5. As for the following figures, values measured on the samples are sorted in ascending order, from low to high, to allow for a progressive visualization of the distribution of the measured

parameters. Vertical black bars show standard deviations from the average values. Measurements spread out in a wide range, with a minimum of 745 m/s and a maximum of 3169 m/s. The average velocity of the whole dataset is 1737 m/s.

5.2. Point load test

The obtained  $I_{S50}$  values are shown (in ascending order) in Fig. 6, for all the 54 tested samples. As already observed for UPV results,  $I_{S50}$  values distribute quite homogeneously over a wide interval (0.02–1.2 MPa), with a high variability of values among the samples. The average  $I_{S50}$  computed based on the whole dataset is 0.44 MPa.

In addition to the obtained  $I_{S50}$  values, macroscopic observation on sample failure during the tests (Fig. 7a) highlighted systematic differences between samples having  $I_{S50}$  lower and higher than

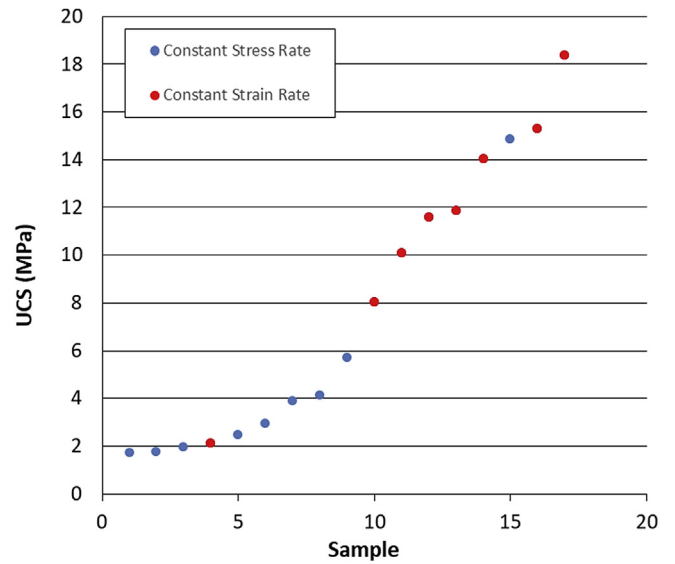


Fig. 8. UCS values determined on 17 samples from UCS tests, sorted in ascending order.

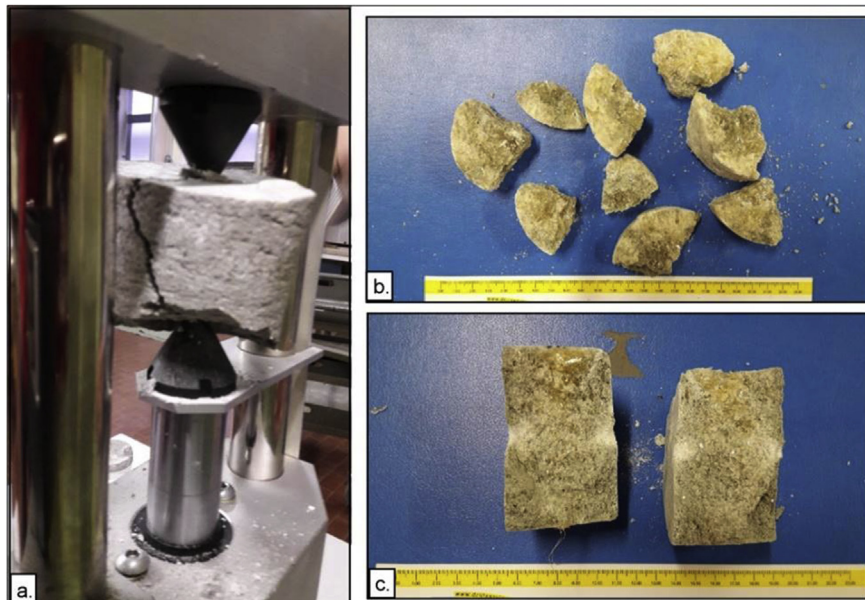


Fig. 7. (a) Macroscopic observations of sample failure during PLTs; (b) Post-failure rock fragments of samples with  $I_{S50}$  values lower than 0.5–0.6 MPa; and (c) Post-failure rock fragments of samples with  $I_{S50}$  values higher than 0.5–0.6 MPa.

0.5–0.6 MPa. In the first case, samples often broke in several scraps, with failure surfaces being developed not only vertically but also sub-horizontally, following the weakness surfaces of the rock anisotropies (Fig. 7b). In the second case, samples generally broke in two parts, with a clear sub-vertical failure surface (Fig. 7c).

5.3. Uniaxial compressive strength test

The UCS values obtained on 17 samples tested with either constant stress rate or constant stress rate procedures are shown in Fig. 8, sorted in ascending order. UCS ranges between 1.73 MPa and 18.35 MPa. Stress–strain curves obtained from the constant stress rate tests are plotted in Fig. 9 and the related elastic parameters are summarized in Table 2. To simplify the reading, samples were labeled from U1 to U8. Elastic parameters referred to the samples U7 and U8 are not presented because, during the test, the strain gages unglued from the samples.

Since electrical strain gages were often unreliable in the post-peak phase, losing cohesion with the sample due to the rock failure or excessive deformation, strain values measured with strain gages and LVDTs were compared. The total strain measured with LVDTs is shown in Fig. 9a. These data provide an estimate of the deformation behavior of the material, both in pre- and post-peak phases (even if the strain is overestimated). For comparison, lateral and axial stress–strain curves obtained with the strain gages, offering a more precise measure of the local deformation, are shown in Fig. 9b. The qualitative comparison between the axial strain curves underlines similar trends within the different measurement methods, highlighting the effectiveness of strain gages on this kind of material. A similar distribution of Young’s modulus–UCS

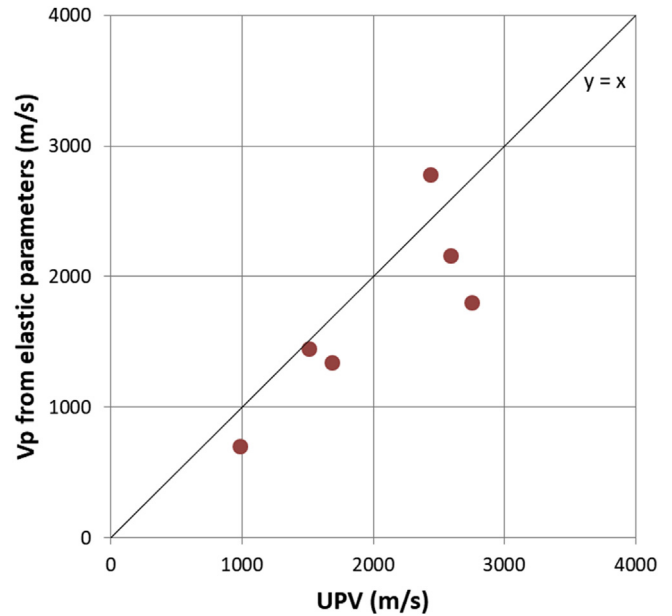


Fig. 10. Comparison among  $V_p$  retrieved from elastic parameters and from the UPV measurements.

values is clear from both graphs. Samples U1, U2, U3 and U8 show UCS and Young’s modulus higher than 11–12 MPa and 6 GPa, respectively. Samples U4, U5 and U7, with UCS between 7 MPa and 12 MPa, have lower Young’s modulus (<3 GPa) and sample U6 has

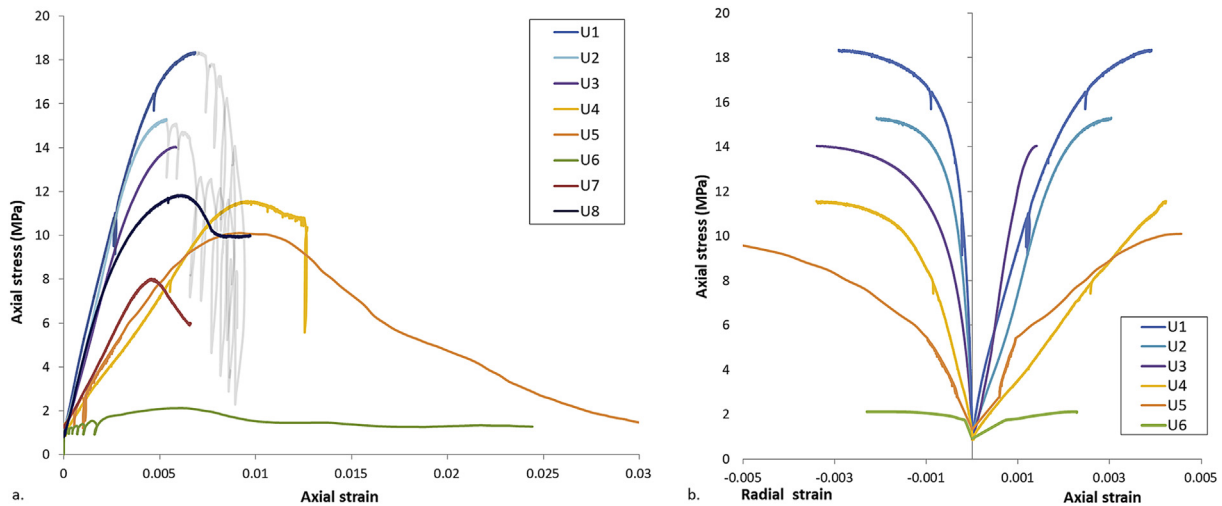
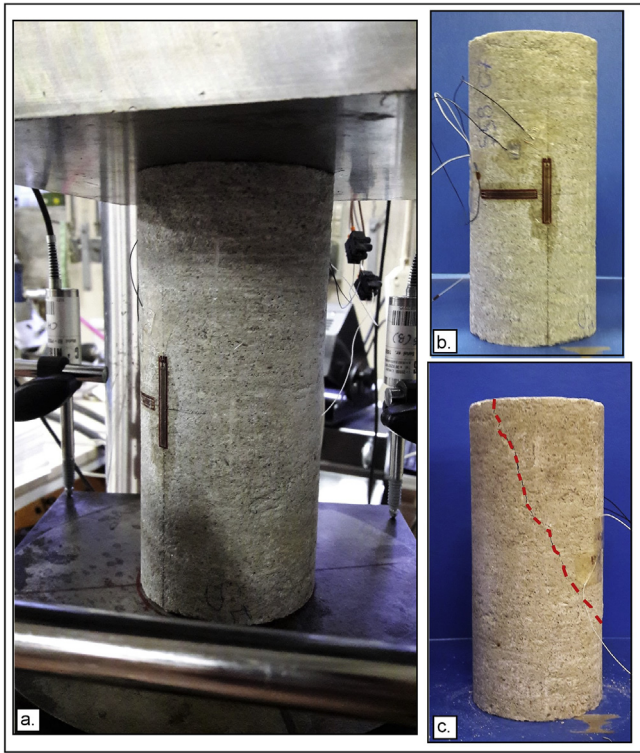


Fig. 9. Stress–strain curves measured with (a) LVDTs and (b) axial and lateral strain gages, for the constant strain rate UCS tests.

**Table 2**  
Summary of the elastic parameters retrieved from constant strain-rate UCS tests. The Young’s modulus and Poisson’s ratio were obtained using the deformation values from the strain gages and by calculating the tangent to the 50% of the stress–strain curve.  $V_p$  values were calculated from the elastic parameters, considering an average density of 2.4 g/cm<sup>3</sup>, and compared with the UPV measured on the same samples.

Sample	Peak strength (MPa)	Ultimate strength (MPa)	Young’s modulus (GPa)	Poisson’s ratio	$V_p$ calculated (m/s)	$V_p$ measured with UPV test (m/s)
U1	18.35		6.68	0.24	1799.82	2753.1
U2	15.3	11.47	7.61	0.33	2158.95	2593.5
U3	14.04		14.47	0.29	2781.54	2434.73
U4	11.57	10.8	2.86	0.37	1442.68	1512.78
U5	10.1	0.23	1.71	0.42	1341.7	1690.3
U6	2.12	1.45	0.8	0.33	698.62	986
U7	8.02	5.89				
U8	11.84	9.98				





**Fig. 11.** (a) Sample tested within the UCS apparatus; (b) before and (c) after the test. In (b), horizontal and vertical electrical strain gages used for the test are shown, and in (c), evidence of the failure surface is depicted.

both UCS and Young’s modulus values much lower than those of all the other samples.

The Young’s modulus and Poisson’s ratio were obtained by using the deformation values from the strain gages and by calculating the tangent to the 50% of the stress–strain curve. From these values, P-wave velocities ( $V_p$ ) were retrieved for a direct comparison with the  $V_p$  measured on the same samples with the UPV test. For the majority of samples, a good correspondence is found between measured UPV values and calculated  $V_p$  (Fig. 10).

In correspondence with the peak load, visible failures were not often observable on the sample surface. The observable growth of the first macroscopic cracks began during the loss of load in the post-peak phases. Cracks progressively propagated until a well-defined failure surface was formed, with an angle of approximately  $50^\circ$ – $60^\circ$  with the core horizontal edges. In most cases, the specimen did not reach a final collapse, but an internal cohesion

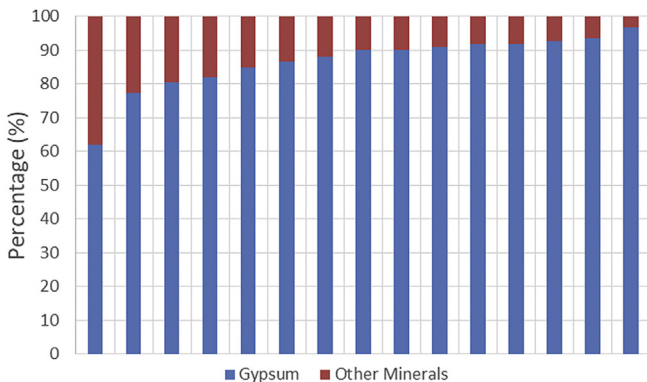


**Fig. 12.** Results of the chemical analyses, sorted in ascending order of gypsum content.

was maintained even after failure (see Fig. 11c). Samples with the lowest strength did not always develop a well-defined failure surface. Conversely, sub-horizontal breaking surfaces, following rock anisotropy direction, were observed. These surfaces seem to develop along the fine material films separating different gypsum lenses.

5.4. Gypsum content measurement

The results of chemical characterization on the 15 analyzed samples report gypsum percentages on the total composition varying between 62% and 97% (Fig. 12). Most of the samples (12) are, however, in a range between 80% and 93%.

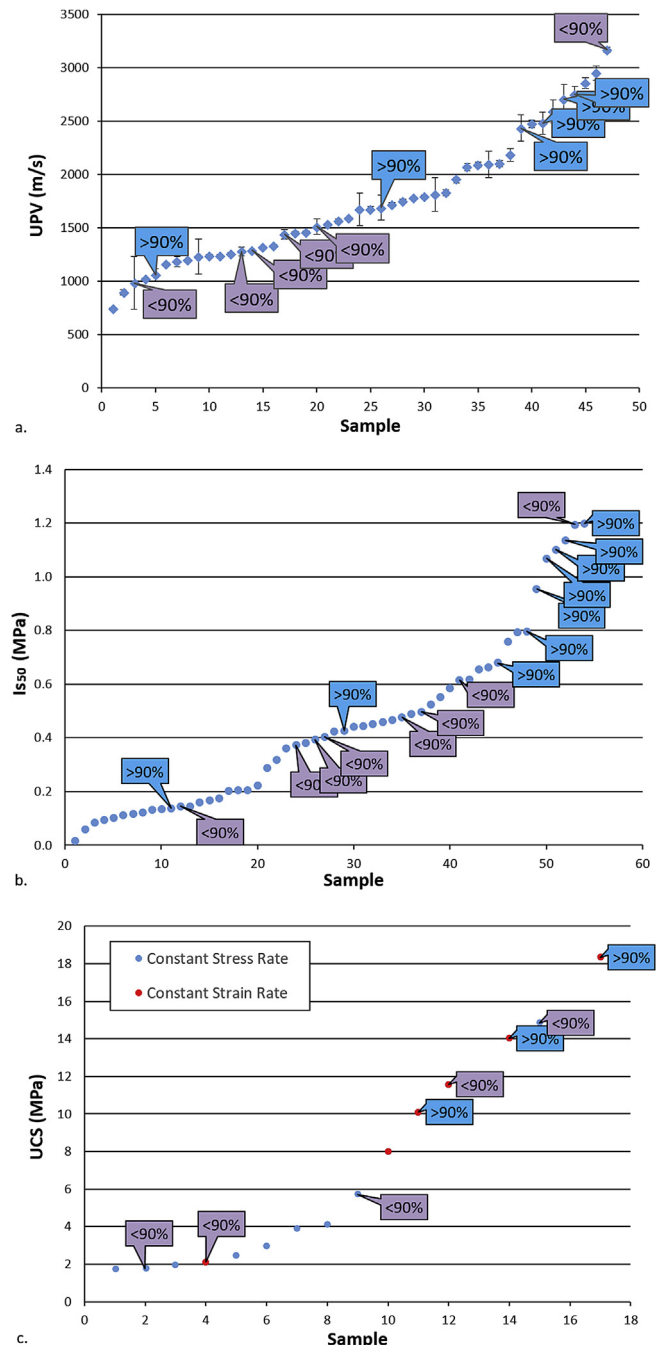


**Fig. 13.** Data of (a) UPV, (b)  $I_{550}$  and (c) UCS, with associated gypsum content (labels).

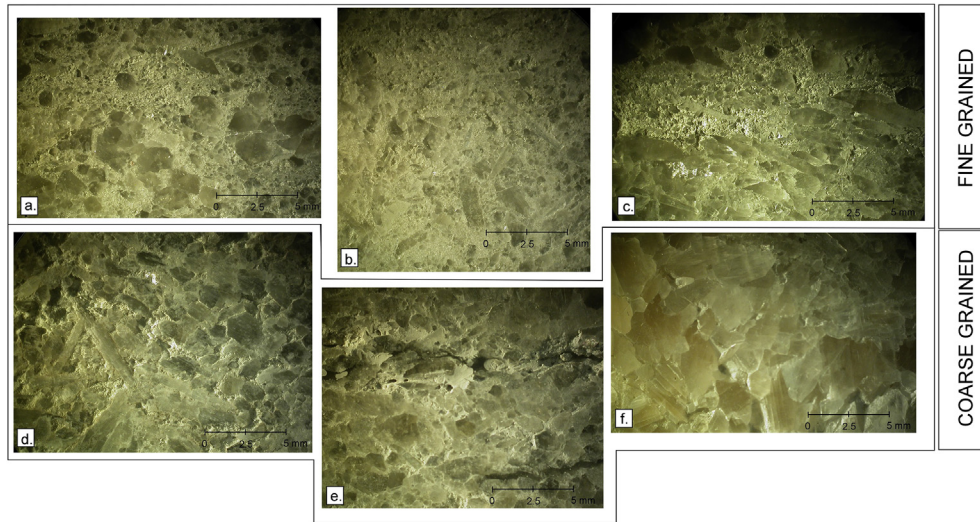


Fig. 14. Thin section photos of the gypsum samples observed with an optical microscope in reflected light.

Gypsum content data, divided in percentage higher and lower than 90%, were overlapped to the results of mechanical characterization in Fig. 13. Despite some outliers, a coherent trend between gypsum percentages and strength data is observed: samples with gypsum content higher than 90% reflect higher mechanical properties (retrieved from direct or indirect measurements), whereas gypsum content lower than 90% corresponds, in general, to lower strength.

5.5. Thin section observation

The analyzed thin sections are shown in Fig. 14. An increase in grain size is noticed from Fig. 14a–f. Two main groups with similar textural features can be recognized, based on qualitative observation and grain size distribution curves (Fig. 15a): fine-grained (Fig. 14a–c) and coarse-grained samples (Fig. 14d–f).

Fine-grained samples show the dominant presence of a matrix of small crystals (around 0.1 mm) that concentrate along layers, elongated in the direction of anisotropy, wrapping oval lenses with 1–2 mm crystals. Some of the gypsum crystals into these lenses show an elongated shape, with the maximum length of 9–10 mm,

underlying the anisotropy (Fig. 14c). In this configuration, crystals are perfectly in contact, without any empty space. This is mainly due to the poor sorting of the grain size and the consequent presence of fine crystals (<0.5 mm) in the void among coarser grains.

Conversely, coarse-grained samples do not show the presence of fine gypsum crystals and the grain size seems to be more homogeneous, resulting in a clast-supported texture. In addition, these sections show a less compact structure, showing thin void spaces among the crystals (Fig. 14d) or the embedded presence of fine marl films, with braided shape and sub-horizontal direction (Fig. 14e). In the coarsest section (Fig. 14f), the most significant feature is the average crystal dimension, locally equal to 3–4 mm, almost twice the average size in the other sections; a few layers with slightly variable grain sizes, parallel to the anisotropy planes, have also been recognized.

The grain size distribution curves and their derivatives (Fig. 15a and b, respectively) confirm that, even if the larger crystals have similar sizes in the two groups (1–2 mm), the fine-grained samples have a significant finer content (0.1–0.5 mm, see the local peak in Fig. 15b), which is not present in the other group.

Porosity estimations (from sample mass in dry and wet conditions) demonstrated that the coarse-grained well-sorted samples

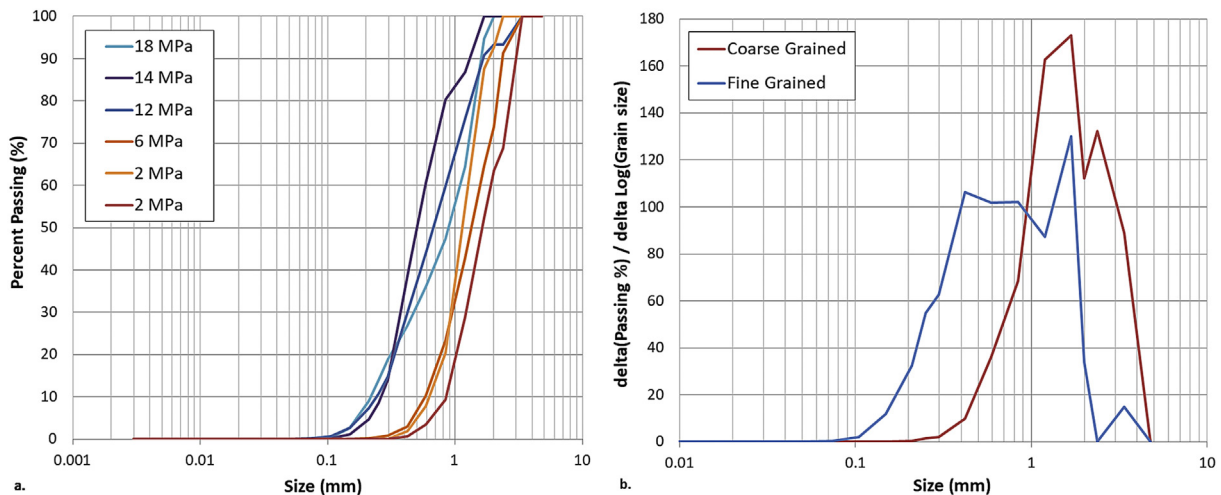


Fig. 15. (a) Grain size distribution curves of the thin sections of Fig. 14; and (b) Derivative of the average curves of the fine and coarse grained classes showing the peaks of the maximum concentration of grain size.

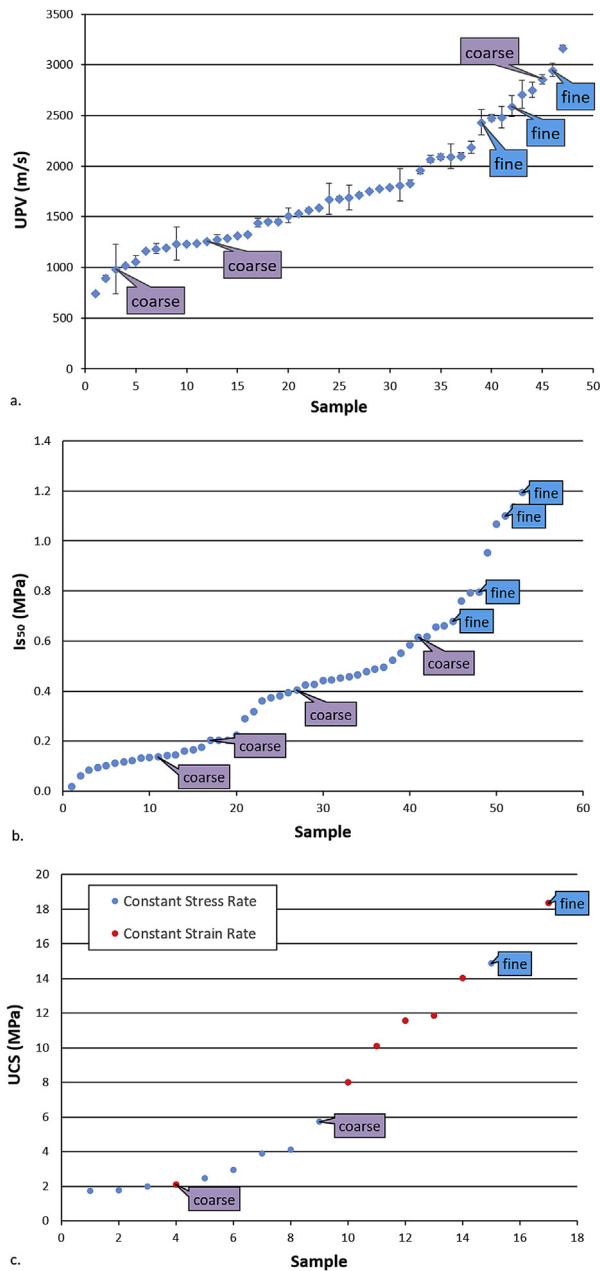


Fig. 16. Data of (a) UPV, (b)  $I_{550}$  and (c) UCS, with associated grain size group (labels).

are indeed characterized by higher porosity values (7%–8%), while the fine-grained poor-sorted samples show lower porosity, usually lower than 5%.

An indication of the grain size group was overlapped to the mechanical parameters (Fig. 16). In general, it can be observed that, similarly to the distribution of chemical indicators, fine-grained materials cluster in the higher part of the graphs, while coarse-grained samples correspond to the lower strength data.

## 6. Discussion

### 6.1. Correlation between mechanical features

Correlations between UCS values and PLT and UPV measurements have been attempted. For these analyses, only one PLT result for each original core was considered.  $I_{550}$ -UCS and UPV-UCS

relationships are shown in Fig. 17 and summarized in Table 3, in terms of linear, exponential and logarithmic regressions. Exponential regression gave the higher correlation coefficient ( $R^2 = 0.97$ ) for  $I_{550}$ -UCS data, while the best fitting for UPV-UCS data was found with linear and logarithmic regressions ( $R^2 = 0.68$  and 0.65, respectively).

In agreement with previous observations on weak rocks (Palchik and Hatzor, 2004; Kahraman et al., 2005; Sabatakakis et al., 2008), the linear correlation factor between PLT and UCS tests has a value approximately half of the standard value ( $UCS/I_{550} = 24.5$ ), which is proposed as a good approximation for all the rock types by ASTM D5731-07 (2007). The strength-dependent relationship between  $I_{550}$  and UCS is confirmed by the best fitting of the measurements with an exponential regression, which should be considered as a general regression curve for the studied facies of gypsum.

Since the compositional and textural variations of the material were likely to have a significant influence on the mechanical behavior (Figs. 13 and 16), two material classes were defined based on chemical indicators and grain size features. To quantitatively describe the coarse and fine-grained materials, we used the parameter  $D_{10}$  (the grain size corresponding to the 10% of passing material), since we noted that the discriminant factor among the two groups of material is the size of finer grains.

The two groups showed different mechanical features and the corresponding mechanical thresholds were identified as  $UCS = 6$  MPa and  $I_{550} = 0.6$  MPa. Consequently, a UPV threshold value has been estimated through the UCS-UPV relationship in Table 3. As a result, a summary of mechanical parameters, composition and grain size for the two material classes is reported in Table 4.

Due to the difference in the geological constituting factors and mechanical features, two UCS- $I_{550}$  specific relationships could potentially more correctly define the two material classes. Data have been therefore preliminarily interpolated by two linear regressions (Fig. 18 and Table 5), with different slopes. Chemical indicators and grain size features are overlapped to the graph, underlining the division. The correlation coefficient of the coarse-grained samples (Class 1) is still high ( $R^2 = 0.9$ ). Even if the correlation coefficient for the fine-grained class (Class 2,  $R^2 = 0.67$ ) is much lower than the one of the exponential interpolation of the entire dataset ( $R^2 = 0.97$ ), the two proposed equations are based on uniformity of features, offering a more realistic representation of the material and avoiding to classify both materials with too high heterogeneity.

### 6.2. Dependence of mechanical behavior from geological features

In Fig. 19, all the results of the compositional analyses are compared to the corresponding UCS values, obtained either directly from the uniaxial tests or from  $I_{550}$  and UPV values, using the relationships proposed in Table 3. The thresholds (gypsum content = 90% and  $UCS = 6$  MPa) used to divide the material classes are highlighted in the graph. Almost all the samples of Class 1 (gypsum content < 90%) fall in the area with  $UCS < 6$  MPa (violet), whereas samples of Class 2 (gypsum content > 90%) mainly fall in the area with  $UCS > 6$  MPa (blue). Only four points fall outside the two classes.

Microscopic observations can help in explaining the occurrence of these outliers: letters referring to the thin sections of Fig. 14 are reported in Fig. 19. Points with  $UCS < 6$  MPa and gypsum content > 90% may be explained by textural and structural observations on the thin section of Fig. 14f. Even if in this sample, the gypsum percentage is the highest among the considered samples (96.7%), extremely low strength values are obtained both from PLT and UPV measurements. This anomalous behavior may be related to the

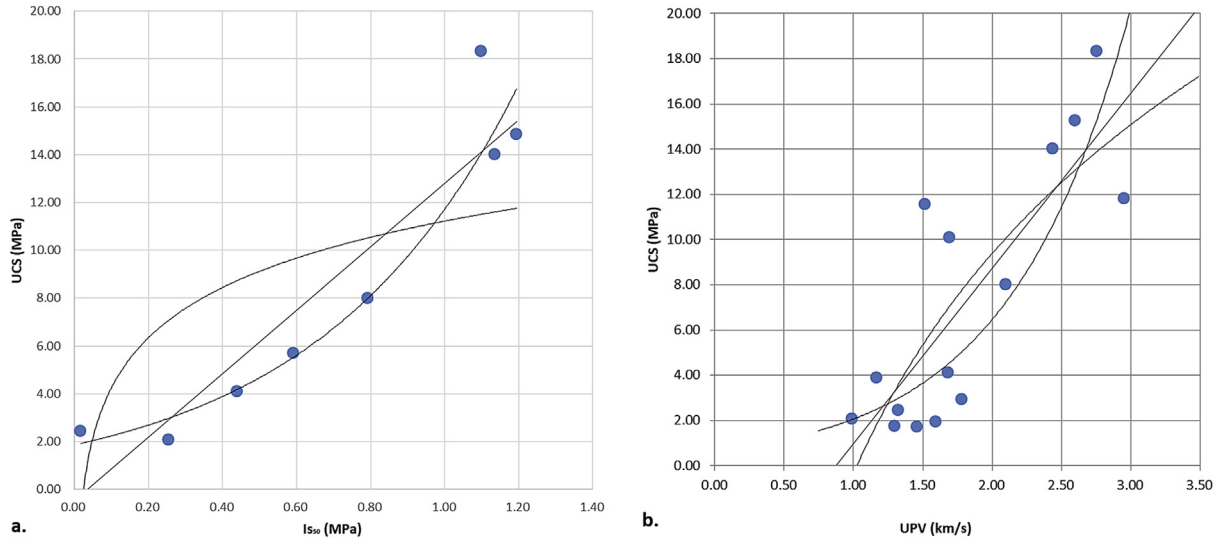


Fig. 17. (a)  $I_{550}$ -UCS and (b) UPV-UCS measurements, with linear, exponential and logarithmic regression curves.

grain size that is coarser and locally almost twice the one observed in the other thin sections, as highlighted from the grain size distribution curve in Fig. 15a. Larger grains and intergranular voids promote the formation of failure surfaces at the grain contacts and result in an average reduced strength of the sample.

Conversely, samples with UCS >6 MPa and gypsum content <90% can be explained by the microstructural observations on the thin section of Fig. 14b and related grain size distribution curve in Fig. 15a. This sample shows the presence of extremely fine-sized interlocked crystals with a very high compact structure. Fine-grained and compacted material among crystals seems therefore to promote the increase in strength.

As observed, a decrease in grain size corresponds to an increase in strength (see Fig. 16). Similarly, the presence of fine-grained layers in coarse material contributes to producing higher mechanical strength. Indeed, poorly-sorted materials showed higher strength than well-sorted samples, since the presence of different

grain sizes allows for a more efficient structural organization, resulting in a lower porosity and a higher rock compactness.

Considering the high heterogeneity of this particular facies with respect to other already investigated gypsum rocks, even if the

Table 3

Summary of  $I_{550}$ -UCS and UPV-UCS relationships, obtained with linear, exponential and logarithmic regressions, with associated coefficients of determination ( $R^2$ ).

Relationship	Equation	$R^2$
UCS- $I_{550}$	$UCS = 1.98 \exp(1.79I_{550})$	0.97
	$UCS = 13.29I_{550} - 0.47$	0.87
	$UCS = 3 \ln I_{550} + 11.22$	0.47
UCS-UPV	$UCS = 7.75UPV - 6.75$	0.68
	$UCS = 14.05 \ln UPV - 0.36$	0.65
	$UCS = 0.66 \exp(1.141UPV)$	0.62

Table 4

Summary of mechanical, compositional and structural thresholds between the two recognized material classes. PLT and UCS values have been obtained by the conjunction point between the two linear regressions in Fig. 18.

Material class	Gypsum content (%)	Grain size, $D_{10}$ (mm)	UPV (m/s)	$I_{550}$ (MPa)	UCS (MPa)
1	<90	0.1–0.2 (coarse)	<1600	<0.65	<6
2	>90	0.5–1 (fine)	>1600	>0.65	>6

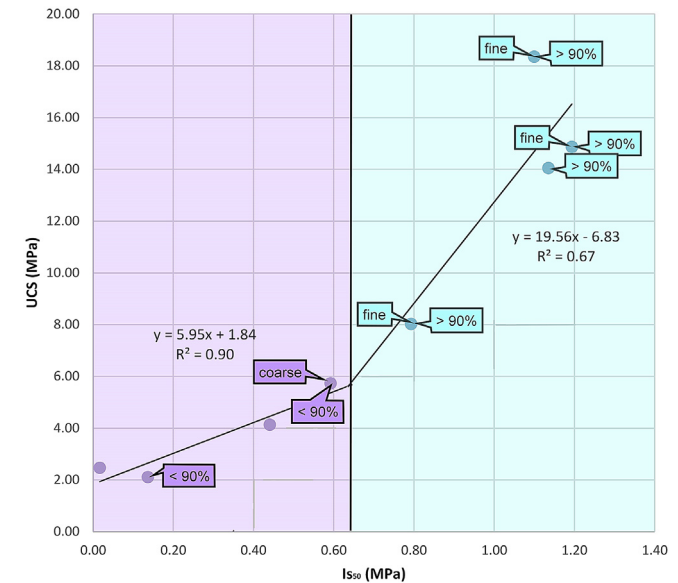
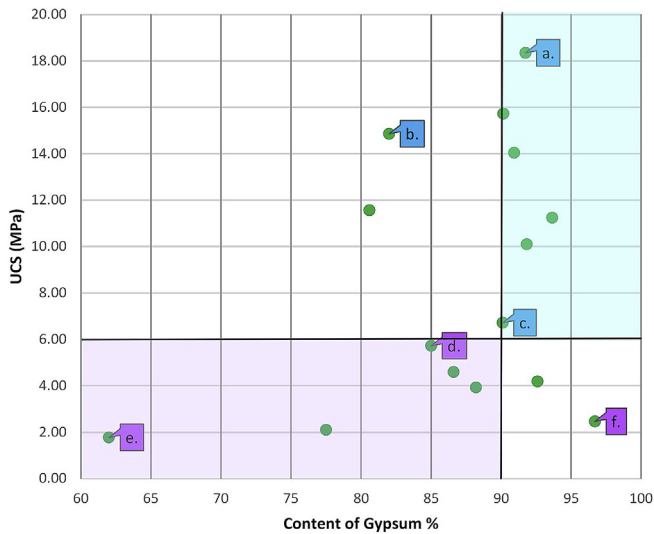


Fig. 18.  $I_{550}$ -UCS relationships based on chemical and textural differences. Labels refer to the percentages of gypsum content and the grain sizes observed in thin sections.

Table 5

$I_{550}$ -UCS relationships, with associated coefficients of determination ( $R^2$ ), for the two identified material classes.

Material class	Equation	$R^2$
1	$UCS = 5.95I_{550} + 1.84$	0.9
2	$UCS = 19.56I_{550} - 6.83$	0.67



**Fig. 19.** Relationship between gypsum content (percentage over the total sample weight) and UCS value, retrieved from either uniaxial tests or PLT and UPV measurements. Letters refer to the subsections in Fig. 14 (microscopic images related to the labeled samples). Violet and blue areas refer to material classes 1 and 2, respectively.

gypsum-content division of the material into two classes well addresses the overall variability of mechanical parameters, microstructural and textural peculiarities should be strongly considered for a complete understanding of the specific material strength.

## 7. Conclusions

Recent geological studies highlighted the presence in the whole Mediterranean basin of different gypsum facies, among which the branching selenite facies was investigated in this study. This facies is considered a key sedimentological level for stratigraphic reconstruction and ore deposit evaluation. Despite the scientific and economical (mining) interest, it has been poorly geologically and mechanically investigated. To fill this gap, this study aimed at evaluating the mechanical properties of this material and proposing specific correlations between standard UCS values and more economical and expeditious tests, such as PLT and UPV measurements. These relationships were established in a general form, disregarding additional information on the sample content and structure, with an exponential law linking PLT results and UCS values and a linear regression for UPV-UCS measurements.

The proposed relationships have to be considered valid only for the specific branching selenite facies. Nevertheless, the basin-scale homogeneous peculiarities of this layer make the results of this work potentially applicable to rock mechanics and engineering geology issues related to this facies all over the Mediterranean Sea.

Despite the choice of focusing on a well-defined gypsum rock type, a large variability of mechanical parameters was detected by all the adopted methods. The related wide range of representative strength values is mainly due to the facies inner heterogeneities (in terms of grain size, composition, textural and structural organization of the crystals) caused by its depositional mechanism.

As a consequence, to further constrain the origin of this mechanical variability, additional information on the grain size and gypsum content was retrieved from representative microscopic and chemical analyses of the tested materials. Although slight strength dependence from the gypsum content was noticed, given a similar gypsum content, the grain size was found to be the key parameter influencing strain features. Two material classes were firstly identified on the basis of these microscopic features, only

partially addressing the dispersion of the mechanical parameters. Further microstructural and textural aspects, linked to the presence of local grain size heterogeneities and to the sorting of the material, were found to complementarily explain the variability in the mechanical behavior.

All these aspects have therefore to be considered for further applications of specific  $I_{550}$ -UCS and UPV-UCS relationships. More in detail, a preliminary subdivision in two linear relationships was adopted for  $I_{550}$ -UCS based on the two recognized material classes and offering new insights into grain size dependent conversion factors for branching selenite gypsum rocks. Nevertheless, given the low number of measurements used to retrieve the proposed correlations, the two introduced linear relationships have to be considered as a preliminary result, to be confirmed and supported by further studies.

Since it was demonstrated that a large variability of mechanical parameters could occur even within the same gypsum facies, the availability of faster and cheaper testing methods (PLT and UPV measurements) and UCS correlations potentially gives access to a larger set of measurements in field applications. This can be considered as a powerful tool to improve the reliability of the material characterization in engineering and mining works, with respect to the limited number of UCS determinations in everyday practice.

Future perspectives of this work include an enrichment of the presented dataset with data on the mineralogical content and microscale observations with transmitted-light microscopy and scanning electron microscopy (SEM). Further analyses on the influence of porosity and natural water content of the material could introduce important modifications in the mechanical behavior.

## Conflicts of interest

We wish to confirm that there are no known conflicts of interest associated with this publication and there has been no significant financial support for this work that could have influenced its outcome.

## Acknowledgements

The authors desire to thank the anonymous private company that kindly provided the core materials for this study.

## References

- Aggastalis G, Alivizatos A, Stamoulis D, Stourmaras G. Correlating uniaxial compressive strength with Schmidt hardness, point load index, Young's modulus, and mineralogy of gabbros and basalts (Northern Greece). *Bulletin of the International Association of Engineering Geology* 1980;22(1):3–11.
- Akram MS, Farooq S, Naeem M, Ghazi S. Prediction of mechanical behaviour from mineralogical composition of Sakesar limestone, Central Salt Range, Pakistan. *Bulletin of Engineering Geology and the Environment* 2017;76(2):601–15.
- Aladejare AE, Wang Y. Evaluation of rock property variability. *Georisk Assessment and Management of Risk for Engineered Systems and Geohazards* 2017;11(1):22–41.
- ASTM D3148-02. Standard test method for elastic moduli of intact rock core specimens in uniaxial compression. West Conshohocken, Pennsylvania, USA: ASTM International; 2002.
- ASTM D2845-08. Standard test method for laboratory determination of pulse velocities and ultrasonic elastic constants of rock. West Conshohocken, Pennsylvania, USA: ASTM International; 2008.
- ASTM D5731-07. Standard test method for determination of the point load strength index of rock and application to rock strength classifications. West Conshohocken, Pennsylvania, USA: ASTM International; 2007.
- Basu A, Kamran M. Point load test on schistose rocks and its applicability in predicting uniaxial compressive strength. *International Journal of Rock Mechanics and Mining Sciences* 2010;47(5):823–8.
- Bernardi E. Integrated stratigraphy of the northernmost record of the Messinian salinity crisis: new insights from the Tertiary Piedmont Basin (PhD Thesis). Turin, Italy: Università degli Studi di Torino; 2013.
- Bieniawski ZT. The point-load test in geotechnical practice. *Engineering Geology* 1975;9(1):1–11.
- Broch E, Franklin JA. The point-load strength test. *International Journal of Rock Mechanics and Mining Sciences* 1972;9(6):669–76.

- Butel N, Alex H, Mehmet SK. Prediction of in situ rock strength using sonic velocity. In: Proceedings of the 14th coal operators' conference, University of Wollongong, The Australasian Institute of Mining and Metallurgy & Mine Managers Association of Australia; 2014. p. 89–102.
- Chau KT, Wong RHC. Uniaxial compressive strength and point load strength of rocks. *International Journal of Rock Mechanics and Mining Sciences and Geomechanics Abstracts* 1996;33(2):183–8.
- Chen Z, Sucech S, Faber KT. A hierarchical study of the mechanical properties of gypsum. *Journal of Materials Science* 2010;45(16):4444–53.
- Clari P, Dela Pierre F, Novaretti A, Timpanelli M. Late oligocene Miocene sedimentary evolution of the critical Alps-Apennine junction: the Monferrato area, northwestern Italy. *Terra Nova* 1995;7:144–52.
- Çobanoğlu İ, Çelik SB. Estimation of uniaxial compressive strength from point load strength, Schmidt hardness and P-wave velocity. *Bulletin of Engineering Geology and the Environment* 2008;67(4):491–8.
- Colombero C, Comina C, Umili G, Vinciguerra S. Multiscale geophysical characterization of an unstable rock mass. *Tectonophysics* 2016;675:275–89.
- Dela Pierre F, Clari P, Cavagna S, Bicchi E. The Parona chaotic complex: a puzzling record of the Messinian (Late Miocene) events in Monferrato (NW Italy). *Sedimentary Geology* 2002;152(3):289–311.
- Dela Pierre F, Festa A, Irace A. Interaction of tectonic, sedimentary, and diapiric processes in the origin of chaotic sediments: an example from the Messinian of Torino hill (Tertiary Piedmont Basin, Northwestern Italy). *Geological Society of America Bulletin* 2007;119(9–10):1107–19.
- Dela Pierre F, Bernardi E, Cavagna S, Clari P, Gennari R, Irace A, Lozar F. The record of the Messinian salinity crisis in the Tertiary Piedmont Basin (NW Italy): the Alba section revisited. *Palaeogeography Palaeoclimatology Palaeoecology* 2011;310(3–4):238–55.
- Dela Pierre F, Clari P, Bernardi E, Natalicchio M, Costa E, Cavagna S, Lozar F. Messinian carbonate-rich beds of the Tertiary Piedmont Basin (NW Italy): microbially-mediated products straddling the onset of the Salinity Crisis. *Palaeogeography Palaeoclimatology Palaeoecology* 2012;344–345:78–93.
- Dela Pierre F, Clari P, Natalicchio M, Ferrando S, Giustetto R, Lozar F, Lugli S, Manzi V, Roveri M, Violanti D. Flocculent layers and bacterial mats in the mudstone interbeds of the primary lower gypsum unit (Tertiary Piedmont Basin, NW Italy): archives of palaeoenvironmental changes during the Messinian salinity crisis. *Marine Geology* 2014;355:71–87.
- Dela Pierre F, Natalicchio M, Lozar F, Bonetto S, Carnevale G, Cavagna S, Colombero S, Sabino M, Violanti D. The northernmost record of the Messinian salinity crisis (Piedmont Basin, NW Italy). *Geological Field Trips* 2016;8:58.
- Eswaran H, Gong ZT. Properties, genesis, classification, and distribution of soils with gypsum. *Soil Science Society of America Special Publication* 1991;26:89–119.
- Everall TJ, Sanislav IV. The influence of pre-existing deformation and alteration textures on rock strength, failure modes and shear strength parameters. *Geosciences* 2018;8:124. <https://doi.org/10.3390/geosciences8040124>.
- Fener M, Kahraman S, Bilgil A, Gunaydin O. A comparative evaluation of indirect methods to estimate the compressive strength of rocks. *Rock Mechanics and Rock Engineering* 2005;38(4):329–43.
- Hardy SJ. The point load test for weak rock in dredging applications. *International Journal of Rock Mechanics and Mining Sciences* 1997;34(3–4). 295.e1–13.
- Hatherly P, Medhurst T, Sliwa R, Turner R. A rock mass assessment procedure based on quantitative geophysical log analysis of coal measure sequences. *Exploration Geophysics* 2005;36(1):112–7.
- Hatherly P, Medhurst T, MacGregor S. A rock mass rating scheme for clastic sediments based on geophysical logs. In: Proceedings of the international workshop on rock mass classification in underground mining; 2007. p. 57–62.
- Hatzor YH, Palchik V. The influence of grain size and porosity on crack initiation stress and critical flaw length in dolomites. *International Journal of Rock Mechanics and Mining Sciences* 1997;34(5):805–16.
- Heidari M, Khanlari GR, Kaveh MT, Kargarian S. Predicting the uniaxial compressive and tensile strengths of gypsum rock by point load testing. *Rock Mechanics and Rock Engineering* 2012;45(2):265–73.
- Hilgen FJ, Krijgsman W, Langereis CG, Lourens LJ, Santarelli A, Zachariasse WJ. Extending the astronomical (polarity) time scale into the Miocene. *Earth and Planetary Science Letters* 1995;136(3–4):495–510.
- ISRM. Suggested method for determining point load strength. *International Society for Rock Mechanics (ISRM)*; 1985.
- JahanGer ZK, Ahmed AA. Correlation between point load index and very low uniaxial compressive strength of some Iraqi rocks. *Australian Journal of Basic and Applied Sciences* 2013;7(7):216–29.
- Ju Y, Yang Y, Peng R, Mao L. Effects of pore structures on static mechanical properties of sandstone. *Journal of Geotechnical and Geoenvironmental Engineering* 2013;139(10):1745–55.
- Kahraman S, Gunaydin O, Fener M. The effect of porosity on the relation between uniaxial compressive strength and point load index. *International Journal of Rock Mechanics and Mining Sciences* 2005;42(4):584–9.
- Kahraman S, Gunaydin O. The effect of rock classes on the relation between uniaxial compressive strength and point load index. *Bulletin of Engineering Geology and the Environment* 2009;68(3):345–53.
- Karakul H, Ulusay R. Empirical correlations for predicting strength properties of rocks from P-wave velocity under different degrees of saturation. *Rock Mechanics and Rock Engineering* 2013;46(5):981–99.
- Karaman K, Kesimal A. Correlation of Schmidt rebound hardness with uniaxial compressive strength and P-wave velocity of rock materials. *Arabian Journal for Science and Engineering* 2015;40(7):1897–906.
- Kaya A, Karaman K. Utilizing the strength conversion factor in the estimation of uniaxial compressive strength from the point load index. *Bulletin of Engineering Geology and the Environment* 2015;75:341–57.
- Lawrence W, Emery J, Canbulat I. Geotechnical roof classification for an underground coal mine from borehole data. In: Proceedings of the 13th coal operators' conference, University of Wollongong, The Australasian Institute of Mining and Metallurgy & Mine Managers Association of Australia; 2013. p. 16–20.
- Li D, Wong LNY. Point load test on meta-sedimentary rocks and correlation to UCS and BTS. *Rock Mechanics and Rock Engineering* 2013;46(4):889–96.
- Liu QS, Zhao YF, Zhang XP. Case study: using the point load test to estimate rock strength of tunnels constructed by a tunnel boring machine. *Bulletin of Engineering Geology and the Environment* 2017. <https://doi.org/10.1007/s10064-017-1198-x>.
- Lugli S, Schreiber C, Tribertp B. Giant polygons in the realmonte mine (Agrigento, Sicily): evidence for the desiccation of a messemian halite basin. *Journal of Sedimentary Research* 1999;69(3):764–71.
- Lugli S, Vinicio M, Roveri M, Schreiber BC. The primary lower gypsum in the Mediterranean: a new facies interpretation for the first stage of the Messinian salinity crisis. *Palaeogeography Palaeoclimatology Palaeoecology* 2010;297(1):83–99.
- Manzi V, Lugli S, Roveri M, Schreiber BC. A new facies model for the upper gypsum of Sicily (Italy): chronological and palaeoenvironmental constraints for the Messinian salinity crisis in the Mediterranean. *Sedimentology* 2009;56(7):1937–60.
- Manzi V, Lugli S, Roveri M, Schreiber BC, Gennari R. The messinian 'calcare di base' (Sicily, Italy) revisited. *Bulletin of the Geological Society of America* 2011;123(1–2):347–70.
- Manzi V, Gennari R, Hilgen F, Krijgsman W, Lugli S, Roveri M, Sierro FJ. Age refinement of the Messinian salinity crisis onset in the Mediterranean. *Terra Nova* 2013;25(4):315–22.
- McNally GM. The prediction of geotechnical rock properties from sonic and neutron logs. *Exploration Geophysics* 1990;21(2):65–71.
- Oyler DC, Mark C, Molinda GM. In situ estimation of roof rock strength using sonic logging. *International Journal of Coal Geology* 2010;83(4):484–90.
- Palchik V, Hatzor YH. The influence of porosity on tensile and compressive strength of porous chalks. *Rock Mechanics and Rock Engineering* 2004;37(4):331–41.
- Papadopoulos Z, Kolaiti E, Mourtzas N. The effect of crystal size on geotechnical properties of neogene gypsum in Crete. *Quarterly Journal of Engineering Geology* 1994;27(3):267–73.
- Piana F, Polino R. Tertiary structural relationships between Alps and Apennines: the critical Torino hill and Monferrato area, northwestern Italy. *Terra Nova* 1995;7:138–43.
- Porta J. Methodologies for the analysis and characterization of gypsum in soils: a review. *Geoderma* 1998;87(1):31–46.
- Rajabzadeh MA, Moosavinasab Z, Rakhshandehroo G. Effects of rock classes and porosity on the relation between uniaxial compressive strength and some rock properties for carbonate rocks. *Rock Mechanics and Rock Engineering* 2012;45(1):113–22.
- Rouchy JM, Caruso A. The Messinian salinity crisis in the Mediterranean basin: a reassessment of the data and an integrated scenario. *Sedimentary Geology* 2006;188–189:35–67.
- Roveri M, Lugli S, Vinicio M, Schreiber BC. The Messinian Sicilian stratigraphy revisited: new insights for the Messinian salinity crisis. *Terra Nova* 2008;20(6):483–8.
- Sabatákakis N, Koukis G, Tsiambaos G, Papanakli S. Index properties and strength variation controlled by microstructure for sedimentary rocks. *Engineering Geology* 2008;97(1–2):80–90.
- Salah H, Omar M, Shanableh A. Estimating unconfined compressive strength of sedimentary rocks in United Arab Emirates from point load strength index. *Journal of Applied Mathematics and Physics* 2014;2(6):296–303.
- Sharma P, Singh T. A correlation between P-wave velocity, impact strength index, slake durability index and uniaxial compressive strength. *Bulletin of Engineering Geology and the Environment* 2008;67(1):17–22.
- Singh TN, Kainthola A, Venkatesh A. Correlation between point load index and uniaxial compressive strength for different rock types. *Rock Mechanics and Rock Engineering* 2012;45(2):259–64.
- Tsiambaos G, Sabatakakis N. Considerations on strength of intact sedimentary rocks. *Engineering Geology* 2004;72(3–4):261–73.
- UNI EN 1926-2007. Natural stone test methods - determination of uniaxial compressive strength. UNI; 2007.
- Vasanelli E, Colangiuli D, Calia A, Sbartai ZM, Breyse D. Combining non-invasive techniques for reliable prediction of soft stone strength in historic masonries. *Construction and Building Materials* 2017;146:744–54.
- Vasconcelos G, Lourenço PB, Alves CAS, Pamplona J. Ultrasonic evaluation of the physical and mechanical properties of granites. *Ultrasonics* 2008;48(5):453–66.
- Wang Y, Li X. Experimental study on cracking damage characteristics of a soil and rock mixture by UPV testing. *Bulletin of Engineering Geology and the Environment* 2015;74:775–88.
- Wasantha PLP, Ranjith PG, Zhao J, Shao SS, Permata G. Strain rate effect on the mechanical behaviour of sandstones with different grain sizes. *Rock Mechanics and Rock Engineering* 2015;48(5):1883–95.
- Weng MC, Li HH. Relationship between the deformation characteristics and microscopic properties of sandstone explored by the bonded-particle model. *International Journal of Rock Mechanics and Mining Sciences* 2012;56:34–43.

- Yasar E, Erdogan Y. Correlating sound velocity with the density, compressive strength and Young's modulus of carbonate rocks. *International Journal of Rock Mechanics and Mining Sciences* 2004;41(5):871–5.
- Yilmaz I, Sendir H. Correlation of Schmidt hardness with unconfined compressive strength and Young's modulus in gypsum from Sivas (Turkey). *Engineering Geology* 2002;66(3):211–9.
- Yilmaz I. Differences in the geotechnical properties of two types of gypsum: alabastrine and porphyritic. *Bulletin of Engineering Geology and the Environment* 2007;66(2):187–95.
- Yu M, Wei CH, Niu LL. The coupled effect of loading rate and grain size on tensile strength of sandstones under dynamic disturbance. *Shock and Vibration* 2017. <https://doi.org/10.1155/2017/6989043>.
- Zel I, Yu T, Ivankina I, Levin DM, Lokajicek T. Application of a modified method of ultrasonic measurements for determination of elastic moduli of rocks. *Crytallography Reports* 2015;60(4):537–45.



**Chiara Caselle** obtained her BSc degree in Geological Science in 2013 and her MSc degree in Geology Applied to Engineering and Environment in 2015 at the Department of Earth Science of at University of Turin, Italy. She is actually a PhD student in the same department, with a research project entitled "Gypsum physical mechanical characterization and innovative surveying methodologies to reduce geological risks in quarry environment". Her research interests include (1) the mechanical behavior of rock materials and the relationship with microstructural, textural and chemical features, (2) the time-dependent behavior of rock materials and (3) the modern technologies for underground safety in quarry environments.



**Sabrina Bonetto** is a researcher at the Department of Earth Science of Torino University. She graduated in Geological Science at Torino University in 2002. She received her PhD in Environmental Engineering at the Politecnico di Torino in April 2006. She has a teaching experience in the fields of Applied Geology, Geoenvironment and Quarry activities. Her research interests involve the research and valorization of mineral resources, the slopes stability and the geomechanical field. She is author and co-author of more than 60 scientific and technical papers on these topics. She participated in national and international research projects carried out at the Department of Earth Sciences of the University of Turin, as well as Research Conventions and technical-scientific consultancy for public and private organizations and companies.



**Chiara Colombero** is a researcher (RTDa) of the Department of Environment, Land and Infrastructure Engineering of Politecnico di Torino since March 2018. She graduated in Geology Applied to Engineering and Environment at the Department of Earth Science of Università degli Studi di Torino in 2012. In the same department, she received her PhD in Earth Sciences with a thesis in Applied Geophysics entitled "Microseismic strategies for characterization and monitoring of a potentially unstable rock mass" in March 2017. She currently works in the Applied Geophysics research group and is teaching assistant in Applied Geophysics, Exploration Geophysics and Applied Geology/Geophysics. Her research interests encompass

seismic and non-seismic methods applied to a wide variety of fields, from rock mass stability to glacier characterization and monitoring, from surface-wave analyses for the detection of subsurface anomalies to geological and hydrogeological investigations in water-covered environments, from engineering geology purposes to archaeological research and cultural heritage preservation and restoration.



**Cesare Comina** is associate professor in applied geophysics at University of Turin. He has also been Research Associate at Politecnico di Torino where he previously graduated in Civil Engineering and awarded of his PhD in Geotechnical Engineering. In the past years, he has carried out his researches at the Department of Structural and Geotechnical Engineering of Politecnico di Torino, where he has collaborated to several funded research projects and participated to the scientific activities of the Geotechnical section. Currently he pertains to the Department of Earth Sciences at University of Turin and collaborates with the group of Applied Geology. He has a teaching experience both in Geophysics and Geotechnics. His researches involve the use of different geophysical

methods for geotechnical and geological characterization. Particularly he has developed innovative testing apparatuses for geophysical monitoring of laboratory tests and he has addressed the use of surface wave tests for dynamic site characterization. He is currently involved in researches related to geothermal energy usage and exploration and he has also worked on waterborne geophysical surveys for the characterization of riverbed or lake sediments. On these topics, he is author and co-author of more than 70 scientific and technical papers both in international journals and conferences.